Cell Reports

Article

Pre-existing subclones determine radioresistance in rectal cancer organoids

Graphical abstract

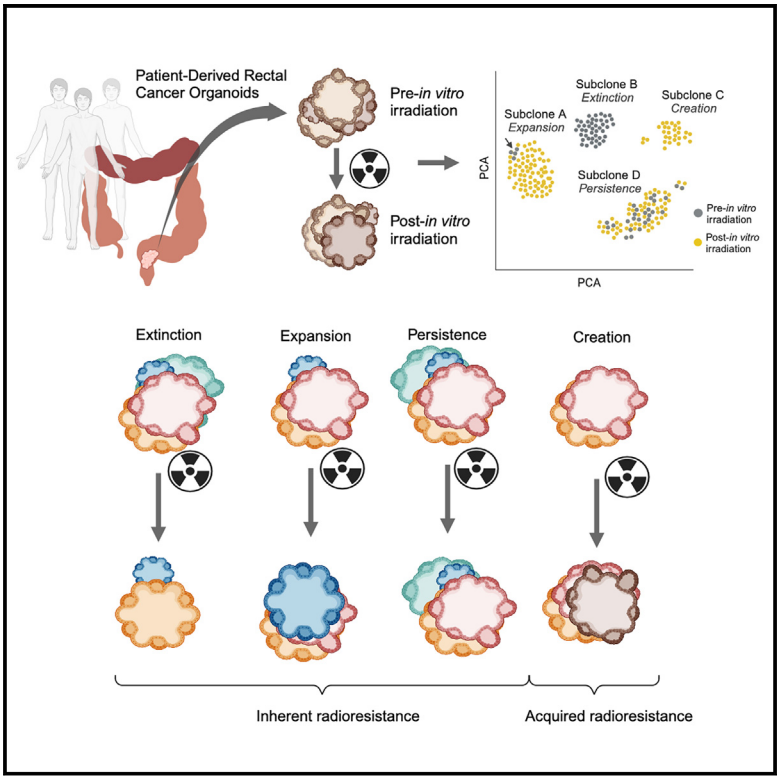

Highlights

- Single-cell sequencing of organoids reveals subclonal dynamics in response to irradiation
- Most radioresistant subclones are present in the organoid culture prior to irradiation
- *De novo* copy-number alterations that expand upon treatment are rare
- Subclonal radioresistance is associated with decreased mitotic chromosomal instability

Authors

Daan Andel, Bas Jeroen Viergever, Niek Alexander Peters, ..., Jeroen Hagendoorn, Inne Hildbrand Max Borel Rinkes, Onno Kranenburg

Correspondence

i.h.m.borelrinkes@umcutrecht.nl (I.H.M.B.R.), o.kranenburg@umcutrecht.nl (O.K.)

In brief

Andel et al. use organoid technology and single-cell karyotype sequencing to track subclonal evolution in response to irradiation. They show that most cancer subclones pre-exist before treatment rather than being newly created (i.e., treatment induced). These results suggest that, in theory, radioresistance may be predicted upfront.

Andel et al., 2024, Cell Reports *43*, 113735
February 27, 2024
https://doi.org/10.1016/j.celrep.2024.113735

CellPress

Cell Reports

CellPress
OPEN ACCESS

Article

Pre-existing subclones determine radioresistance in rectal cancer organoids

Daan Andel,[1,2] Bas Jeroen Viergever,[2] Niek Alexander Peters,[1,2] Danielle Adriana Elisabeth Raats,[2] Susanne Jolien Schenning-van Schelven,[2] Martijn Peter Willem Intven,[3] Maurice Zandvliet,[4] Jeroen Hagendoorn,[1,2] Inne Hildbrand Max Borel Rinkes,[1,2,*] and Onno Kranenburg[1,2,5,6,*]

[1]Department of Surgical Oncology, University Medical Center Utrecht, Cancer Center, Utrecht, the Netherlands
[2]Laboratory for Translational Oncology, University Medical Center Utrecht, Cancer Center, Utrecht, the Netherlands
[3]Department of Radiation Oncology, University Medical Center Utrecht, Cancer Center, Utrecht, the Netherlands
[4]Department of Clinical Sciences - Companion Animals, Faculty of Veterinary Medicine, Utrecht University, Utrecht, the Netherlands
[5]Utrecht Platform for Organoid Technology, Utrecht University, Utrecht, the Netherlands
[6]Lead contact
*Correspondence: i.h.m.borelrinkes@umcutrecht.nl (I.H.M.B.R.), o.kranenburg@umcutrecht.nl (O.K.)
https://doi.org/10.1016/j.celrep.2024.113735

SUMMARY

More than half of all patients with cancer receive radiation therapy, but resistance is commonly observed. Currently, it is unknown whether resistance to radiation therapy is acquired or inherently present. Here, we employed organoids derived from rectal cancer and single-cell whole-genome sequencing to investigate the long-term evolution of subclones in response to radiation. Comparing single-cell whole-genome karyotypes between *in-vitro*-unirradiated and -irradiated organoids revealed three patterns of subclonal evolution: (1) subclonal persistence, (2) subclonal extinction, and (3) subclonal expansion. Organoids in which subclonal shifts occurred (i.e., expansion or extinction) became more resistant to radiation. Although radioresistant subclones did not share recurrent copy-number alterations that could explain their radioresistance, resistance was associated with reduced chromosomal instability, an association that was also observed in 529 human cancer cell lines. These data suggest that resistance to radiation is inherently present and associated with reduced chromosomal instability.

INTRODUCTION

Radiation therapy constitutes a cornerstone of cancer treatment, but resistance poses a major clinical challenge. For example, more than 70% of patients with esophageal[1] and rectal cancer[2] receiving chemoradiation therapy have residual disease. Gaining a better understanding of the mechanisms underlying resistance could potentially optimize the efficacy of radiation therapy and aid in the identification of patients who are most likely to respond.

Genomic studies in various malignancies have revealed that resistance to systemic therapy can arise through *de novo* (e.g., treatment-induced) genomic aberrations[3–5] or may be inherently present, such as through the selection of (rare) pre-existing subclones.[3,6,7] Deciphering these mechanisms of resistance is important because if it is indeed inherently present, response to therapy could potentially be predicted by analyzing pre-treatment biopsies.

Many of these studies have used bulk genome sequencing to infer subclonal relationships in response to cancer treatment. However, bulk genomic sequencing lacks the ability to resolve intratumor heterogeneity at a high resolution. As such, the existence of pre-existing rare subclones may go unnoticed. In contrast, single-cell whole-genome sequencing has emerged as a powerful tool enabling the reconstruction of phylogenetic trees[8] and the detection of rare subclones.[9,10]

In the field of radiotherapy, research on this topic has been impeded by challenges in obtaining serial patient samples over time and the lack of suitable *in vitro* models. Recently, organoids have emerged as robust cancer models that can accurately predict clinical responses to radiation therapy in rectal cancer.[11,12] Additionally, organoids recapitulate the genomic intratumor heterogeneity at the single-cell level,[13] making them a powerful model for studying resistance to radiation.

Currently, it remains unknown if resistance to radiation therapy is treatment induced through the generation of *de novo* genomic aberrations or inherently present via the selection of (rare) pre-existing subclones. To address this question, we utilized patient-derived organoids from rectal cancer and employed single-cell whole-genome sequencing to track subclonal evolution in response to radiation.

RESULTS

Patient-derived organoids from rectal cancer display heterogeneous responses to radiation therapy

Eight patient-derived organoids from primary rectal cancers were established, covering all non-*in-situ* AJCC stages.

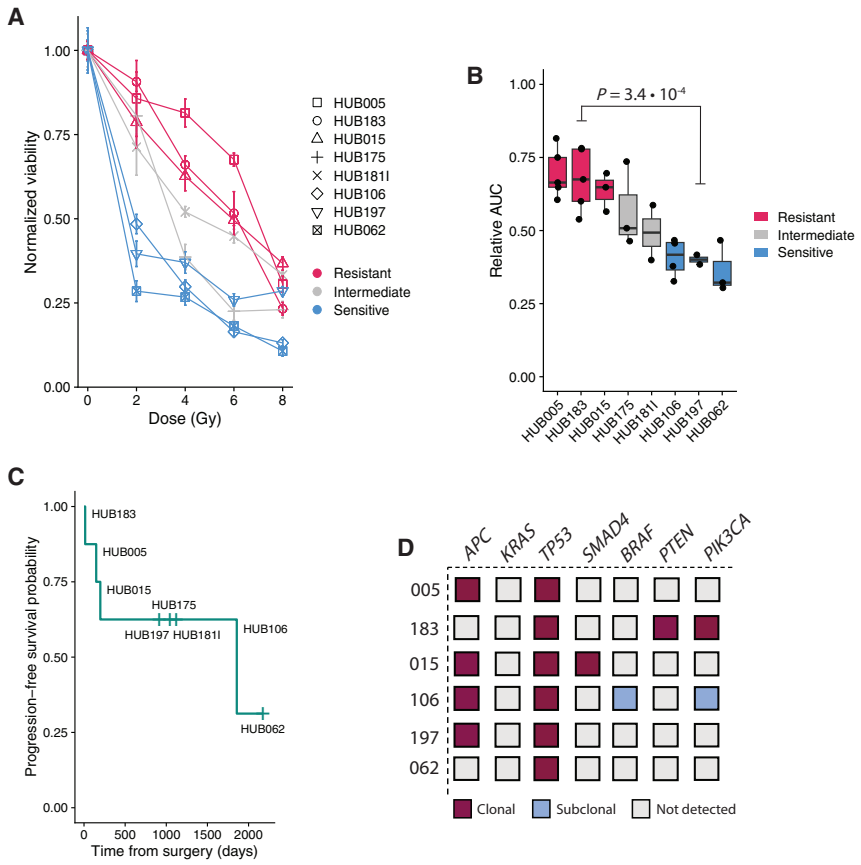

Figure 1. Heterogeneous *in vitro* response to radiation associates with progression-free survival

(A) Representative dose-response plot showing responses (normalized to 0 Gy) of eight rectal-cancer-derived organoids. Data are represented as mean ± SEM.

(B) Combined analysis of the relative area under the curve (AUC) of multiple independent experiments (each dot) reveals low interexperiment variability and identifies three radioresistant organoids (red) and three radiosensitive organoids (blue). p value indicates significance between radioresistant and radiosensitive groups. Welch's two-sample t test after pooling biological experiments for each organoid.

(C) Progression-free survival from the time of surgery (and organoid harvest) for each rectal cancer organoid demonstrates that patients corresponding to resistant organoids progressed early, while patients from whom sensitive organoids were derived had no progression (censored, vertical line).

(D) Oncoplot revealing mutation status of commonly mutated colorectal cancer driver genes for each organoid at baseline.

Table S1 provides detailed information on the basic clinical and tumor characteristics of these organoids. Out of eight organoids, two were derived from patients who received neoadjuvant chemoradiotherapy (HUB183 and HUB181I), while the remaining six were from treatment-naive patients. Next, a high-throughput radiation response assay was utilized, which closely mimics radiation response parameters of the classic clonogenic survival assay in cell lines,[14,15] and was adapted for compatibility with three-dimensional (3D) organoid models (STAR Methods). Briefly, organoids were grown for 3 days in basement membrane extract (BME) microdroplets and exposed to a range of clinically relevant radiation doses. After 7 days, post-radiation cell viability was assessed using CellTiter-Glo 3D, which quantifies intracellular ATP. Differences in sensitivities to radiation therapy were observed between models derived from different patients (Figure 1A). Based on the median values of the area under the curve, three organoids were consistently resistant to radiation (HUB005, HUB183, and HUB015), while three organoids were consistently sensitive (HUB106, HUB197, and HUB062) to radiation, in multiple independently performed experiments (Figure 1B; $p = 3.4 \cdot 10^{-4}$).

In vitro organoid chemoradiation responses correlate with clinical progression-free survival.[11,16] In this study, a statistical correlation between *in vitro* radiation resistance and progression-free survival could not be performed due to censoring of data (i.e., no progression occurred). However, patients with *in vitro* radioresistant organoids (HUB005, HUB183, HUB015) all progressed early after surgery (after 148, 14, and 198 days, respectively), while patients corresponding to radiosensitive organoids (HUB106, HUB197, HUB062) had no progression after 1,857 (died), 917, and 2,175 days, respectively (Figure 1C). Based on these data, three radioresistant organoids (HUB005, HUB183, and HUB015) and three radiosensitive organoids (HUB106, HUB197, HUB062) were selected for further analysis.

Radioresistant and radiosensitive organoids have colorectal-cancer-specific driver mutations and copy-number profiles

To identify mutations in driver genes common to colorectal cancer, targeted genotyping of frequently mutated cancer genes or whole-exome sequencing was performed. This revealed mutations in *TP53* (6/6), *APC* (4/6), *SMAD4* (1/6), *PTEN* (1/6), and *PIK3CA* (1/6) (Figures 1D; Tables S2 and S3). We additionally identified subclonal mutations in HUB106 in $PIK3CA^{E542Q}$ (3.5% variant allele frequency [VAF]) and $BRAF^{V600E}$ (2.2% VAF).

Sparse (~0.1×) single-cell whole-genome sequencing showed that most of the organoids (5 out of 6) exhibited high frequencies of arm- or chromosome-level copy-number alterations, which is also frequently observed in samples from patients with colorectal cancer.[17] Analysis of the single-cell karyotype data showed the presence of several colorectal-cancer-specific arm-level copy-number gains, such as 1q, 7, 8, 13, and 20 p and q, as well as deletions in 18q and 8p, consistent with patient data from TCGA database.[17] HUB015 was the only organoid that was largely diploid, which is apparent in approximately 16% of colorectal cancers.[17,18] HUB197 displayed cells that likely arose from a

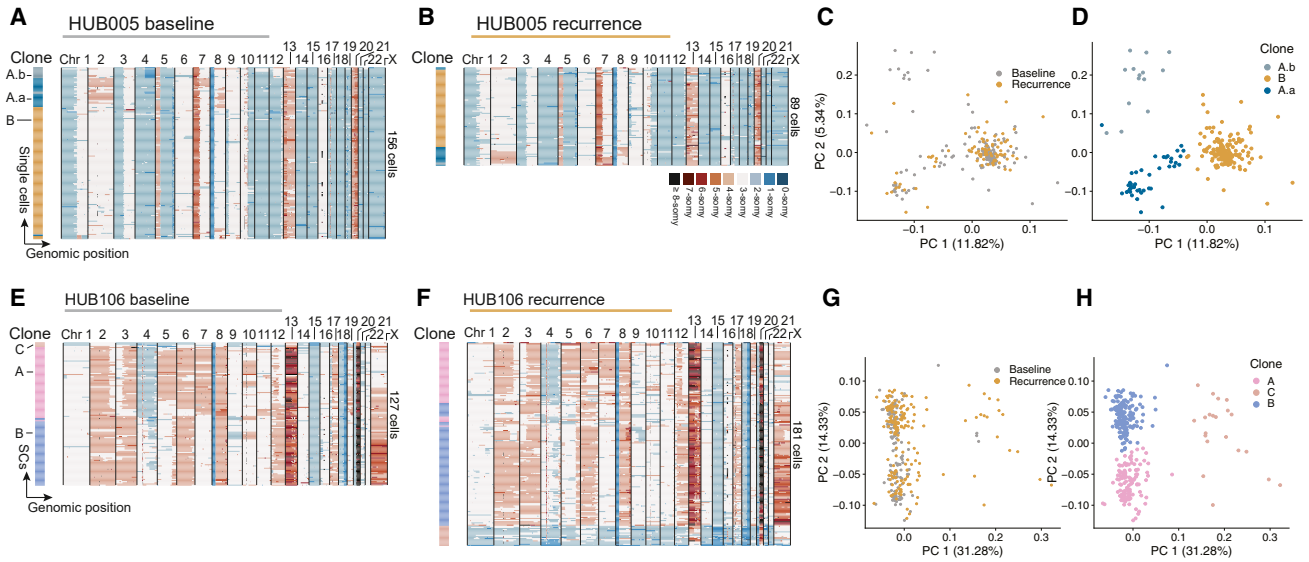

Figure 2. Subclonal evolution in response to irradiation in persister organoids

(A and B) Clustered heatmaps of single-cell copy-number profiles of HUB005 (resistant, persister) at baseline (A) and after recurrence following 10 Gy irradiation (B).

(C and D) Principal-component analysis (PCA) plots of single-cell copy-number profiles from the baseline and recurrence populations. Colors indicate treatment status (C) or subclone (D) as defined using k-means clustering. Major subclones (STAR Methods) are depicted with capital letters, while minor subpopulations within clones are indicated with a suffix (.a, .b, etc.).

(E and F) Cluster heatmaps of single-cell copy-number profiles of HUB106 (sensitive, persister) at baseline (E) and after recurrence following 10 Gy irradiation (F).

(G and H) PCA plots of single-cell copy-number profiles from the baseline and recurrence populations. SCs, single cells.

whole-genome duplication event, as these cells had exactly twice the ploidy of another set of cells within the organoid culture.[19,20]

Distinct modes of subclonal dynamics in response to radiation

Cancer cells may survive therapeutic pressures through inherent or acquired (e.g., treatment-induced) genetic alterations.[3–5,7,21,22] To delineate the subclonal evolution in response to radiation, organoids were subjected to either 0 or 10 Gy radiation. Single-cell whole-genome karyotypes of *in-vitro*-unirradiated organoids (referred to as "baseline") were compared to *in-vitro*-irradiated organoids after they were amenable to passaging (referred to as "recurrence"). Note that organoid HUB183 was derived from a patient who had received prior radiation therapy. Therefore, the baseline sample of this organoid will be referred to as "baseline (PR)," i.e., prior radiotherapy.

Recurrence following 10 Gy was observed after 31 ± 12 days in resistant organoids and after 49 ± 24 days in sensitive organoids. Targeted genotyping revealed no new mutations in cancer driver genes. Furthermore, all clonal mutations were identified before *in vitro* radiation persisted, whereas the subclonal mutations in HUB106 in *PIK3CA*^{E542Q} and *BRAF*^{V600E} were not detected after recurrence (Table S3). Next, the genetic information of single cells obtained at baseline and at recurrence was plotted on the same graph using principal-component analysis. This way, cells with similar copy-number alterations before and after *in vitro* treatment are part of the same subclone and thus cluster together. This allowed detection of pre-existing subclones that persisted or expanded upon treatment. Conversely, post-therapy cells with treatment-induced *de novo* genomic aberrations will form distinct clusters that are not in the vicinity of pre-therapy cells. It was reasoned that cells with a set of similar copy-number alterations should only be considered as part of a formal "major" subclone when the copy-number alterations explained more than 10% of the variance within a principal component (STAR Methods). Clearly separated clusters with less than or equal to 10% of the variance explained were defined as "minor" subclones.

Using this approach, an average of 2.3 major subclones per organoid were identified. Except for diploid organoid HUB015, there was a satisfactory concordance between the inferred subclones using our method and the clonal architecture revealed by MEDICC2, a tool for inferring phylogenies from somatic copy-number alterations (Figures S1 and S2).[23] Three different patterns of major subclonal evolution in response to radiation were observed: (1) subclonal persistence, where the subclones persisted after treatment (Figure 2; Figure S3), (2) subclonal extinction, wherein pre-existing subclones died out following treatment (Figure 3), and (3) subclonal expansion, wherein a pre-existing subclone expanded (Figure 4). Although radiation increased the total number of copy-number alterations (Figure S4) (23), *de novo* copy-number alterations shared by more than 50% of cells were rare. Only in HUB015 was a distinctive new deletion spanning 4q21.21–4q22.2 detected, giving rise to a minor (A.a) subclone emerging from the major subclone A (Figures 4A–4D).

Notably, subclonal persistence was observed in two out of three resistant organoids; subclonal extinction and subclonal expansion were seen in two out of three sensitive organoids.

For example, HUB005, a resistant organoid, had two major subclones (A and B) at baseline, with A subdivided in two minor subclones, A.a (4q diploid) and A.b (4q deletion) (Figures 2A–2D).

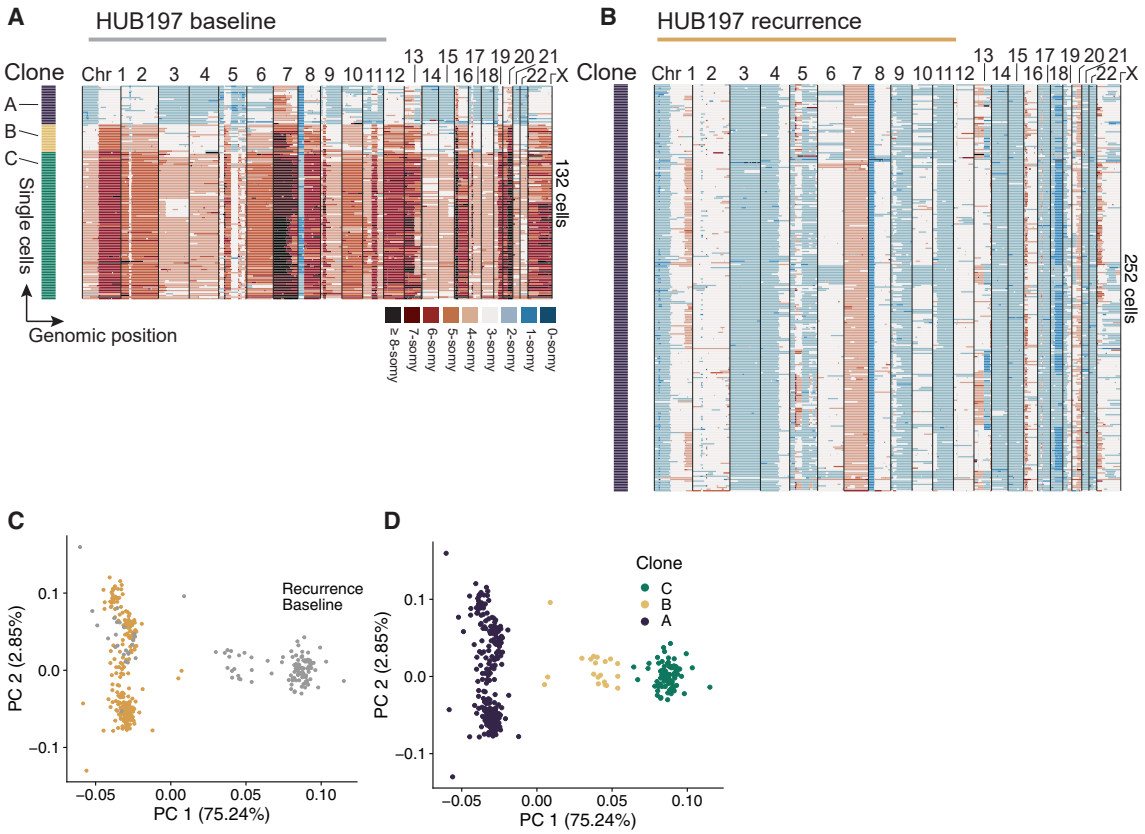

Figure 3. Subclonal evolution in extinction organoid

(A and B) Single-cell copy-number heatmaps of HUB197 (sensitive organoid) at baseline (A) and after recurrence following 10 Gy irradiation (B).

(C and D) PCA plots of single-cell copy-number profiles from the baseline and recurrence populations with colors indicating treatment status (C) or subclone (D).

Upon radiation, all subclones persisted in equal proportions (Fisher's exact test, p = 1, Bonferroni corrected). Persistence was also seen in HUB106 (Figures 2E–2H) and HUB183 (Figure S3). On the other hand, HUB197 (sensitive), which initially had three major subclones at baseline, experienced complete extinction of two subclones ($p = 1.99 \cdot 10^{-71}$; Figure 3). Subclonal expansion was observed in HUB015, where subclone B expanded (from 1 to 14 cells, $p = 6.8 \cdot 10^{-3}$; Figures 4A–4D). Lastly, in HUB062, a radiosensitive organoid, there was a subclone (subclone HUB062A) that constituted only 1.5% of all cells at baseline but expanded upon radiation to make up 47% of all cells at recurrence ($p = 1.56 \cdot 10^{-17}$; Figures 4E and 4F). An independent repeat experiment also showed an aggressive expansion of HUB062A, with complete extinction of subclones HUB062B and HUB062C (Figure S5). Moreover, treating the recovered HUB062 again with 10 Gy resulted in complete dominance of the expansion subclone HUB062A in two independent experiments (from 47% to 100%, Fisher's exact test, $p < 1.16 \cdot 10^{-26}$; Figures 4F–4I).

Subclonal shifts alter sensitivity to radiation

It was hypothesized that organoids that survived therapy and exhibited evidence of subclonal persistence would retain their inherent radioresistance. On the other hand, organoids that showed evidence of subclonal extinction or subclonal expansion were expected to exhibit increased resistance due to shifts favoring radioresistant subclones. Indeed, HUB197 (extinction) and HUB062 (expander) showed increased resistance to radiation compared to their parental counterparts (Figure 5A). In contrast, the resistance of three persister controls (HUB005, HUB183, HUB106) did not change (Figure 5B).

Copy-number alterations associated with radiation resistance

Copy-number alterations may harbor genes that confer a survival benefit to cancer cells when amplified or deleted. Resistance-associated copy-number alterations were identified by computing consensus copy-number alterations for each subclone and selecting only those alterations that were not frequently present in sensitive subclones (STAR Methods). Determining such resistance-specific copy-number alterations revealed that expansion subclone HUB062A, when compared to HUB062B and HUB062C, had unique copy-number amplifications containing oncogenes previously linked to radioresistance, including chromosome-arm 9p (containing proto-oncogenes *JAK2* and *FANCG*), 11p (*FANCF* and *DDB2*), and Xp11.22-Xq23 (*AR*) (Figure 4F, bottom; Table S4). The Fanconi anemia complementation group family of genes are involved in DNA

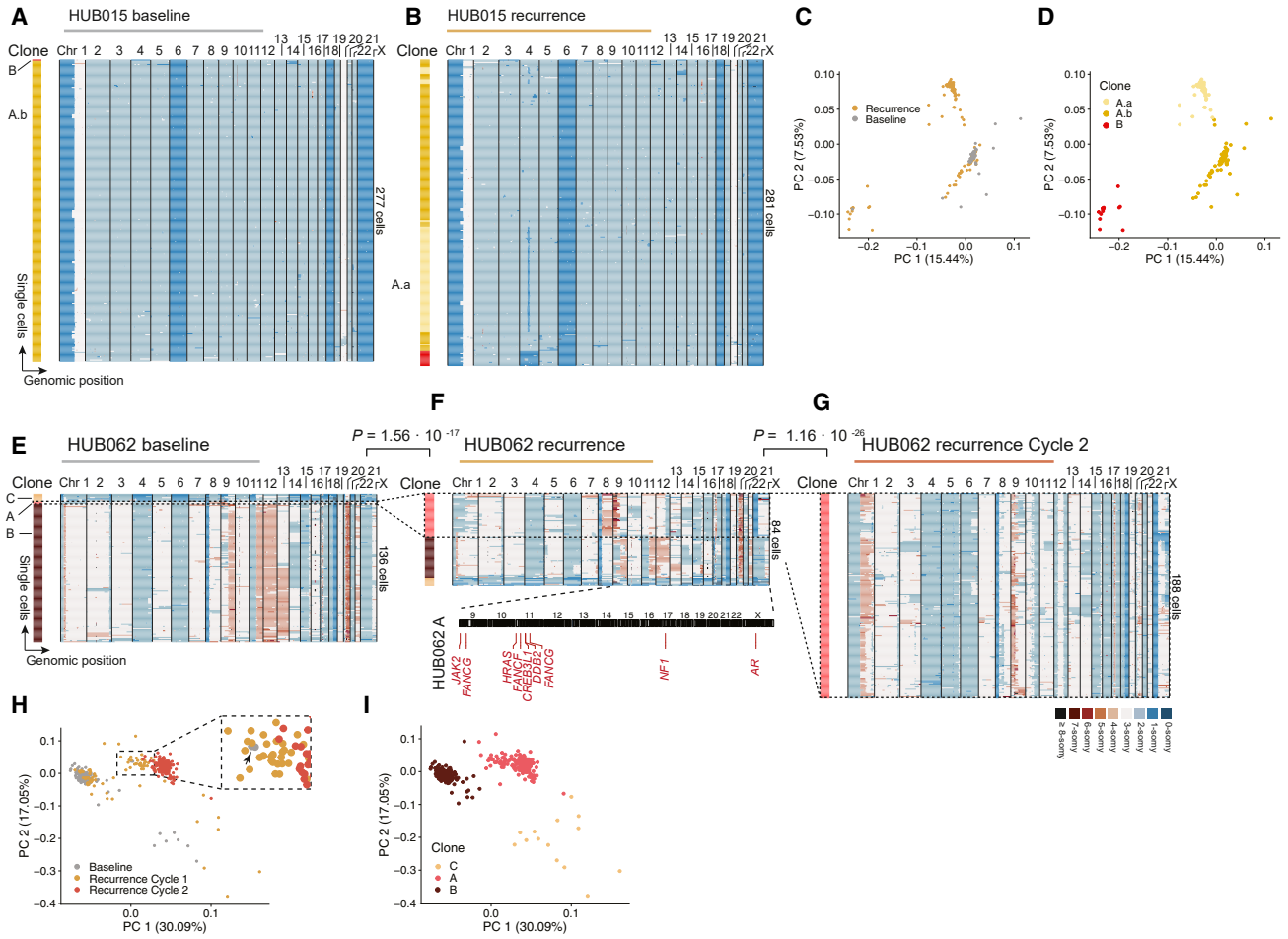

Figure 4. Subclonal evolution in expansion organoids

(A and B) Cluster heatmaps of single-cell copy-number profiles of HUB015 (resistant, persister) at baseline (A) and after recurrence following 10 Gy irradiation (B).

(C and D) PCA plots of single-cell copy-number profiles from the baseline and recurrence populations. Major subclones (STAR Methods) are depicted with capital letters, while minor subpopulations within clones are indicated with a suffix (.a, .b, etc.).

(E–G) Cluster heatmaps of single-cell copy-number profiles of HUB062 (sensitive, expander) at baseline (E), after recurrence following 10 Gy irradiation (F), and after recurrence following another cycle of 10 Gy irradiation (G). (F) Bottom shows the karyotype plot of expansion clone HUB062A with amplified cancer genes specific to HUB062A (when compared to HUB062B and HUB062C).

(H and I) PCA plots of single-cell copy-number profiles from the baseline, recurrence, and recurrence cycle 2 populations. Inset in (H) localizes two cells of subclone HUB062A at baseline (arrowhead). p values are from Fisher's exact test.

interstrand crosslink repair pathways.[24] The acquired deletion in HUB015 on 4q21.21–4q22.2 contained the putative tumor-suppressor gene *PTPN13*, coding a protein tyrosine phosphatase,[25] and proto-oncogene *AFF1*, a transcription elongation factor.[26] Next, we obtained gene-level copy-number calls made by the ABSOLUTE algorithm of 529 cancer cell lines from the Cancer Cell Line Encyclopedia (CCLE) for which radiation sensitivity data were available.[15] In the top 20% radioresistant cell lines, 15.4% had a deletion of *PTPN13*, while only 4.9% of the 20% most radiosensitive cell lines had the deletion ($p = 5.9 \cdot 10^{-3}$, corrected for cancer [sub]type). *AFF1* was also more frequently deleted in radioresistant cell lines than in radiosensitive cell lines (15.4% vs. 3.9%, $p = 4.0 \cdot 10^{-3}$).

However, no specific copy-number alterations shared by all radioresistant subclones were found, indicating that additional mechanisms played a role in explaining subclonal radioresistance.

Radioresistant subclones have copy-number patterns associated with decreased mitotic chromosomal instability

To better understand why some subclones showed resistance to radiation, the single-cell karyotype data were carefully reexamined. Radiosensitive subclones within HUB062, HUB106, and HUB197 had more large- to whole-chromosome copy-number changes compared to other subclones. Additionally, subclones HUB197B and HUB197C—which did not survive after radiation therapy—exhibited whole-genome duplication.[19,20] MEDICC2 revealed the presence of whole-genome duplication events in HUB197, as well as in HUB106, but not in radioresistant

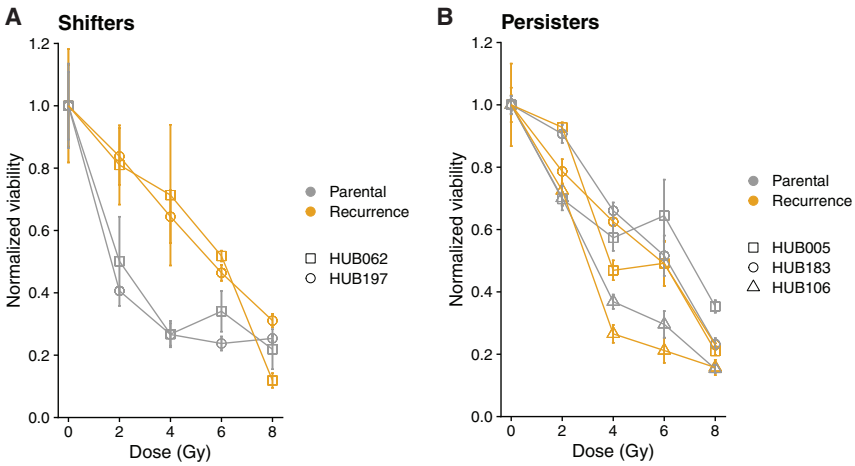

Figure 5. Subclonal shifts alter sensitivity to radiation

(A) Representative dose-response plot showing responses to irradiation between parental and recurrence lines in organoids where subclonal shifts were apparent (HUB062, HUB197).

(B) Dose-response plot in subclonal persisters (HUB106, HUB183, and HUB005). Viability was normalized to 0 Gy. Data are represented as mean ± SEM. n = 3 independent experiments.

organoids. Both these observations hint toward increased ongoing mitotic chromosome segregation errors within these sensitive subclones. To test this hypothesis, cell-to-cell copy-number variability, a measure of chromosomal instability, was assessed within each subclone, as well as arm- to whole-chromosome-level copy-number alterations. Arm- to whole-chromosome-level copy-number alterations are suggestive of chromosomal instability due to mitotic errors.[27] This analysis revealed that sensitive subclones were indeed more heterogeneous (Student's t test, $p = 1.6 \cdot 10^{-2}$; Figure 6A). Moreover, averaging the pairwise distances inferred from MEDICC2 within each subclone similarly revealed higher intraclone variability in radiosensitive organoids, although this difference was not statistically significant (Figure 6B; $p = 2.3 \cdot 10^{-1}$). Finally, cells within sensitive subclones harbored more copy-number alterations, especially at the arm- to whole-chromosome-level (Mann-Whitney U test, $p = 1.4 \cdot 10^{-63}$ and $4.2 \cdot 10^{-83}$; Figure 6C).

Next, ploidy and whole-genome duplication calls were analyzed from the CCLE database, and the top 20% radioresistant and 20% radiosensitive cancer cell lines were compared. In this dataset, neither ploidy (2.71 in radioresistant vs. 2.43 in radiosensitive, $p = 0.11$) nor whole-genome duplication (65 vs. 42%, $p = 0.31$) was significantly associated with radiation sensitivity after correcting for cancer (sub)type. To obtain a more granular view of chromosomal instability, recently published chromosomal instability signatures—each with a different putative cause—were computed for the CCLE cancer cell lines.[27] After correcting for cancer (sub)type, we found that two (2/17) signatures were significantly different when comparing the top 20% radioresistant to the top 20% radiosensitive cancer cell lines. Signature CX1—related to arm or whole-chromosome changes due to mitotic errors and/or telomere dysfunction—was increased in sensitive cell lines ($p = 3.5 \cdot 10^{-2}$; Figure 6D; Table S5), while CX7 (unknown etiology; $p = 6.6 \cdot 10^{-3}$) was decreased.[27]

DISCUSSION

In the present study, we tracked subclonal evolution in response to radiation therapy using rectal cancer patient-derived organoids and single-cell whole-genome sequencing. We observed subclonal persistence, subclonal extinction, or subclonal expansion upon radiation therapy, but the creation of new, commonly shared genomic aberrations was rare. Radiosensitive subclones exhibited copy-number patterns indicative of mitotic segregation errors. This suggests that subclones may be selected based on decreased chromosomal instability.

The results presented here align with previous studies in patients with breast cancers who are treated with a combination of mitotic inhibitors and anthracyclines, which induce DNA damage. These studies have shown that pre-existing subclones can either expand or go extinct, but new subclones are not generated.[6,21] In our study, five out of six analyzed rectal cancer organoids exhibited widespread arm- or chromosome-level copy-number alterations at baseline (i.e., before *in vitro* irradiation), suggesting chromosomal instability.[17] We surmise that chromosomal instability allows the generation of subclones with copy-number alterations that confer a survival benefit upon external pressures.[28] However, we found no copy-number alterations harboring amplified or deleted genes that could comprehensively explain the observed radioresistance of subclones, warranting similar analyses in larger studies in the future.

Although the existence of pre-existing subclones could potentially lead to resistance through their selection and expansion, the data presented here also suggest that increased mitotic chromosomal instability is associated with increased sensitivity to radiation therapy. While we did not observe an association with global proxies of chromosomal instability such as ploidy and whole-genome duplication in the CCLE database, a more granular analysis revealed that radioresistance may be associated with decreased chromosomal instability due to mitotic segregation errors and/or telomere dysfunction. This association with mitotic chromosomal instability is supported by studies showing that suppressing mitotic chromosomal instability can increase resistance to radiation[29] and that patients with high pre-treatment chromosomal instability have better response rates to chemoradiation therapy.[30] The association may be explained by the fact that radiation itself induces mitotic segregation errors,[29,31] thus overwhelming the cell's capacity to cope with the resulting genetic abnormalities.[32]

Interestingly, subclonal persistence was predominantly seen in radioresistant organoids (2/3), while subclonal expansion was observed in two out of three radiosenstive organoids. Although radiation can cause numerous copy-number

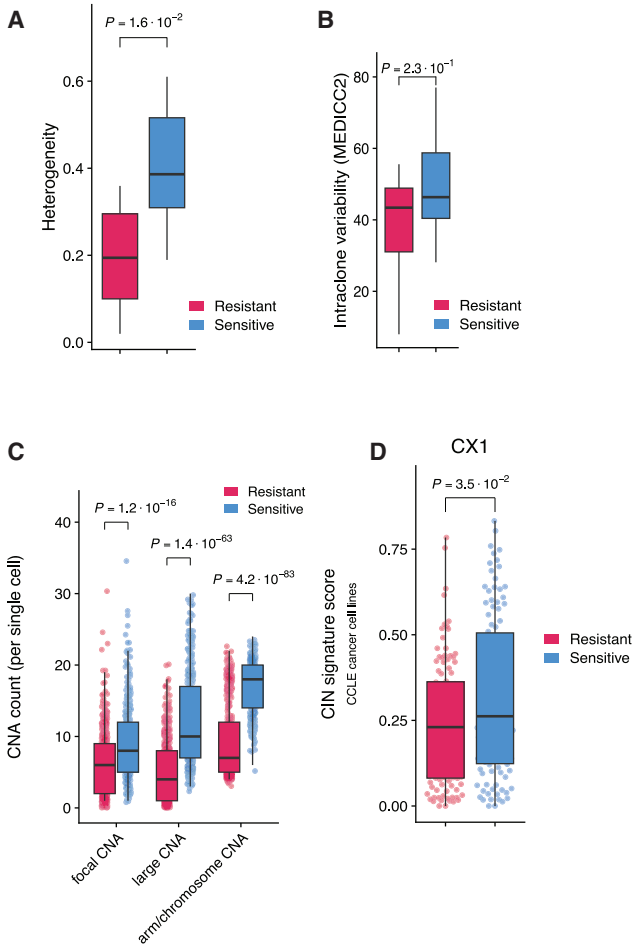

Figure 6. Radioresistance is associated with copy-number patterns suggestive of mitotic chromosomal instability

(A) Heterogeneity score for resistant (red) vs. sensitive (blue) subclones. p values from Student's t test.

(B) Mean of cell-to-cell pairwise distances (MEDICC2 output) within subclones. p values from Student's t test.

(C) Copy-number alteration counts (stratified into focal-, large-, and arm- to whole-chromosome-level size) in single cells from resistant or sensitive subclones. Mann-Whitney U test.

(D) Chromosomal instability signature "CX1" scores from cell lines in the top 20% radioresistant (red) vs. the top 20% radiosensitive (blue) cancer cell lines from the CCLE database. p values from Mann-Whitney U test. CNA, copy-number alteration; CIN, chromosomal instability.

alterations through poorly repaired DNA breaks,[33] we only observed one case of a newly acquired copy-number alteration (4q21.21–4q22.2 deletion) shared by more than 50% of the cells. This *de novo* copy-number alteration arose within subclone HUB015A, giving rise to minor subclone HUB015A.a. This deletion contained *PTPN13*, encoding a protein tyrosine phosphatase non-receptor with putative tumor-suppressor function in solid cancers including colorectal cancer,[25] and proto-oncogene *AFF1*, a leukemogenic gene associated with acute lymphoblastic leukemia when fused with *KMT2A*.[26] While both *PTPN13* and *AFF1* have as of yet not been linked to influencing radioresistance, we found that radioresistant cancer cell lines harbored more *PTPN13* and *AFF1* deletions than radiosensitive lines. We surmise that the deletion in 4q21.21–4q22.2 may have been under positive selection, but future studies in larger samples are necessary to substantiate this hypothesis. Even though irradiation increased the total number of alterations, we found no other newly acquired copy-number alterations that were selected. It appears that radiation-induced alterations are difficult to select for, possibly because other radiation-induced alterations can be harmful to the cell's survival.

The findings presented here appear to indicate that resistance to radiation therapy is largely determined by pre-existing radioresistant subclones that either persist or expand rather than being newly created. This implies that, in theory, radioresistance could be predicted by careful analysis of pre-treatment biopsies, ideally using techniques that can resolve intratumor heterogeneity at great resolution. Analysis of copy-number patterns also indicates that mitotic chromosomal instability may be a biomarker for response to radiation therapy.

Limitations of the study

In this study, most organoids were derived from treatment-naive tumors, except the radioresistant HUB183 organoid, which was derived from a tumor that had been exposed to chemoradiation clinically. Possibly, the radioresistant phenotype of this organoid observed *in vitro* may have resulted from the selective pressure of this prior treatment in the patient. While this study suggests that resistance to radiation appears to be primarily determined by genetic factors that are inherently present, resistance on the epigenetic or transcriptional level may be acquired, and these processes do not necessarily exclude each other.[6] Cell-autonomous factors appear to be important drivers of radioresistance, as indicated by the strong correlation between the radiation response of organoids *in vitro* and clinical response.[11,12] Nevertheless, further research on patient samples is necessary to account for the effects of the microenvironment on subclonal evolution.

STAR★METHODS

Detailed methods are provided in the online version of this paper and include the following:

- KEY RESOURCES TABLE
- RESOURCE AVAILABILITY
  - Lead contact
  - Materials availability
  - Data and code availability
- EXPERIMENTAL MODEL AND SUBJECT PARTICIPANT DETAILS
  - Patient-derived tissue and clinical data
  - Patient-derived tumor organoid culturing
- METHOD DETAILS
  - Radiation response assays
  - Bulk genome sequencing
  - Subclonal evolution modeling
  - Single-cell whole genome sequencing
  - Single-cell sequencing data processing
  - Clustering of subclones
  - Resistance-specific copy number analysis

- Copy number pattern analysis
- Whole genome doubling and ploidy calls
- Chromosomal instability signature

- QUANTIFICATION AND STATISTICAL ANALYSIS

SUPPLEMENTAL INFORMATION

Supplemental information can be found online at https://doi.org/10.1016/j.celrep.2024.113735.

ACKNOWLEDGMENTS

The authors would like to express their gratitude to Geert Kops and Nico Lansu for their valuable scientific insights and code sharing and Joshua Peterson and Floris Leendert for their support during the single-cell experiments. Special gratitude goes toward André Wopereis, Wilfred de Vries, Ingrid Boots, Marjolijn Gross, and Masha de Koning-Hoogeboom for their practical insights and assistance with the irradiation of organoids. This research was funded by a private fund.

AUTHOR CONTRIBUTIONS

D.A. conceived the study and performed experiments, wrote the code and analyzed the data, and wrote the original manuscript. B.J.V., N.A.P., D.A.E.R., and S.J.S.-v.S. performed experiments. M.P.W.I. and M.Z. provided resources. J.H. conceived and supervised the study. I.H.M.B.R. conceived and supervised the study and secured funding. O.K. conceived and supervised the study, wrote the original manuscript, and secured funding. All authors provided expertise and feedback throughout the project and reviewed and edited the manuscript.

DECLARATION OF INTERESTS

The authors declare no competing interests.

Received: September 28, 2023
Revised: December 5, 2023
Accepted: January 17, 2024

REFERENCES

1. Geh, J.I., Crellin, A.M., and Glynne-Jones, R. (2001). Preoperative (neoadjuvant) chemoradiotherapy in oesophageal cancer. Br. J. Surg. *88*, 338–356. https://doi.org/10.1046/j.1365-2168.2001.01670.x.
2. Hoendervangers, S., Couwenberg, A.M., Intven, M.P.W., van Grevenstein, W.M.U., and Verkooijen, H.M. (2018). Comparison of pathological complete response rates after neoadjuvant short-course radiotherapy or chemoradiation followed by delayed surgery in locally advanced rectal cancer. Eur. J. Surg. Oncol. *44*, 1013–1017. https://doi.org/10.1016/j.ejso.2018.03.014.
3. Ding, L., Ley, T.J., Larson, D.E., Miller, C.A., Koboldt, D.C., Welch, J.S., Ritchey, J.K., Young, M.A., Lamprecht, T., McLellan, M.D., et al. (2012). Clonal evolution in relapsed acute myeloid leukaemia revealed by whole-genome sequencing. Nature *481*, 506–510. https://doi.org/10.1038/nature10738.
4. Kim, H., Zheng, S., Amini, S.S., Virk, S.M., Mikkelsen, T., Brat, D.J., Grimsby, J., Sougnez, C., Muller, F., Hu, J., et al. (2015). Whole-genome and multisector exome sequencing of primary and post-treatment glioblastoma reveals patterns of tumor evolution. Genome Res. *25*, 316–327. https://doi.org/10.1101/gr.180612.114.
5. Patch, A.-M., Christie, E.L., Etemadmoghadam, D., Garsed, D.W., George, J., Fereday, S., Nones, K., Cowin, P., Alsop, K., Bailey, P.J., et al. (2015). Whole–genome characterization of chemoresistant ovarian cancer. Nature *521*, 489–494. https://doi.org/10.1038/nature14410.
6. Kim, C., Gao, R., Sei, E., Brandt, R., Hartman, J., Hatschek, T., Crosetto, N., Foukakis, T., and Navin, N.E. (2018). Chemoresistance Evolution in Triple-Negative Breast Cancer Delineated by Single-Cell Sequencing. Cell *173*, 879–893.e13. https://doi.org/10.1016/j.cell.2018.03.041.
7. Kurtova, A.V., Xiao, J., Mo, Q., Pazhanisamy, S., Krasnow, R., Lerner, S.P., Chen, F., Roh, T.T., Lay, E., Ho, P.L., and Chan, K.S. (2015). Blocking PGE2-induced tumour repopulation abrogates bladder cancer chemoresistance. Nature *517*, 209–213. https://doi.org/10.1038/nature14034.
8. Navin, N., Kendall, J., Troge, J., Andrews, P., Rodgers, L., McIndoo, J., Cook, K., Stepansky, A., Levy, D., Esposito, D., et al. (2011). Tumour evolution inferred by single-cell sequencing. Nature *472*, 90–94. https://doi.org/10.1038/nature09807.
9. Martelotto, L.G., Baslan, T., Kendall, J., Geyer, F.C., Burke, K.A., Spraggon, L., Piscuoglio, S., Chadalavada, K., Nanjangud, G., Ng, C.K.Y., et al. (2017). Whole-genome single-cell copy number profiling from formalin-fixed paraffin-embedded samples. Nat. Med. *23*, 376–385. https://doi.org/10.1038/nm.4279.
10. Lohr, J.G., Adalsteinsson, V.A., Cibulskis, K., Choudhury, A.D., Rosenberg, M., Cruz-Gordillo, P., Francis, J.M., Zhang, C.-Z., Shalek, A.K., Satija, R., et al. (2014). Whole-exome sequencing of circulating tumor cells provides a window into metastatic prostate cancer. Nat. Biotechnol. *32*, 479–484. https://doi.org/10.1038/nbt.2892.
11. Ganesh, K., Wu, C., O'Rourke, K.P., Szeglin, B.C., Zheng, Y., Sauvé, C.E.G., Adileh, M., Wasserman, I., Marco, M.R., Kim, A.S., et al. (2019). A rectal cancer organoid platform to study individual responses to chemoradiation. Nat. Med. *25*, 1607–1614. https://doi.org/10.1038/s41591-019-0584-2.
12. Yao, Y., Xu, X., Yang, L., Zhu, J., Wan, J., Shen, L., Xia, F., Fu, G., Deng, Y., Pan, M., et al. (2020). Patient-Derived Organoids Predict Chemoradiation Responses of Locally Advanced Rectal Cancer. Cell Stem Cell *26*, 17–26.e6. https://doi.org/10.1016/j.stem.2019.10.010.
13. Kopper, O., de Witte, C.J., Lõhmussaar, K., Valle-Inclan, J.E., Hami, N., Kester, L., Balgobind, A.V., Korving, J., Proost, N., Begthel, H., et al. (2019). An organoid platform for ovarian cancer captures intra- and interpatient heterogeneity. Nat. Med. *25*, 838–849. https://doi.org/10.1038/s41591-019-0422-6.
14. Abazeed, M.E., Adams, D.J., Hurov, K.E., Tamayo, P., Creighton, C.J., Sonkin, D., Giacomelli, A.O., Du, C., Fries, D.F., Wong, K.-K., et al. (2013). Integrative Radiogenomic Profiling of Squamous Cell Lung Cancer. Cancer Res. *73*, 6289–6298. https://doi.org/10.1158/0008-5472.CAN-13-1616.
15. Yard, B.D., Adams, D.J., Chie, E.K., Tamayo, P., Battaglia, J.S., Gopal, P., Rogacki, K., Pearson, B.E., Phillips, J., Raymond, D.P., et al. (2016). A genetic basis for the variation in the vulnerability of cancer to DNA damage. Nat. Commun. *7*, 11428. https://doi.org/10.1038/ncomms11428.
16. Ooft, S.N., Weeber, F., Dijkstra, K.K., McLean, C.M., Kaing, S., van Werkhoven, E., Schipper, L., Hoes, L., Vis, D.J., van de Haar, J., et al. (2019). Patient-derived organoids can predict response to chemotherapy in metastatic colorectal cancer patients. Sci. Transl. Med. *11*, eaay2574. https://doi.org/10.1126/scitranslmed.aay2574.
17. Cancer Genome Atlas Network (2012). Comprehensive molecular characterization of human colon and rectal cancer. Nature *487*, 330–337. https://doi.org/10.1038/nature11252.
18. Weisenberger, D.J., Siegmund, K.D., Campan, M., Young, J., Long, T.I., Faasse, M.A., Kang, G.H., Widschwendter, M., Weener, D., Buchanan, D., et al. (2006). CpG island methylator phenotype underlies sporadic microsatellite instability and is tightly associated with BRAF mutation in colorectal cancer. Nat. Genet. *38*, 787–793. https://doi.org/10.1038/ng1834.
19. Carter, S.L., Cibulskis, K., Helman, E., McKenna, A., Shen, H., Zack, T., Laird, P.W., Onofrio, R.C., Winckler, W., Weir, B.A., et al. (2012). Absolute quantification of somatic DNA alterations in human cancer. Nat. Biotechnol. *30*, 413–421. https://doi.org/10.1038/nbt.2203.
20. Zack, T.I., Schumacher, S.E., Carter, S.L., Cherniack, A.D., Saksena, G., Tabak, B., Lawrence, M.S., Zhsng, C.Z., Wala, J., Mermel, C.H., et al.

(2013). Pan-cancer patterns of somatic copy number alteration. Nat. Genet. *45*, 1134–1140. https://doi.org/10.1038/ng.2760.

21. Venizelos, A., Engebrethsen, C., Deng, W., Geisler, J., Geisler, S., Iversen, G.T., Aas, T., Aase, H.S., Seyedzadeh, M., Steinskog, E.S., et al. (2022). Clonal evolution in primary breast cancers under sequential epirubicin and docetaxel monotherapy. Genome Med. *14*, 86. https://doi.org/10.1186/s13073-022-01090-2.
22. Bhang, H.e.C., Ruddy, D.A., Krishnamurthy Radhakrishna, V., Caushi, J.X., Zhao, R., Hims, M.M., Singh, A.P., Kao, I., Rakiec, D., Shaw, P., et al. (2015). Studying clonal dynamics in response to cancer therapy using high-complexity barcoding. Nat. Med. *21*, 440–448. https://doi.org/10.1038/nm.3841.
23. Kaufmann, T.L., Petkovic, M., Watkins, T.B.K., Colliver, E.C., Laskina, S., Thapa, N., Minussi, D.C., Navin, N., Swanton, C., Van Loo, P., et al. (2022). MEDICC2: whole-genome doubling aware copy-number phylogenies for cancer evolution. Genome Biol. *23*, 241. https://doi.org/10.1186/s13059-022-02794-9.
24. Webster, A.L.H., Sanders, M.A., Patel, K., Dietrich, R., Noonan, R.J., Lach, F.P., White, R.R., Goldfarb, A., Hadi, K., Edwards, M.M., et al. (2022). Genomic signature of Fanconi anaemia DNA repair pathway deficiency in cancer. Nature *612*, 495–502. https://doi.org/10.1038/s41586-022-05253-4.
25. Wang, Z., Shen, D., Parsons, D.W., Bardelli, A., Sager, J., Szabo, S., Ptak, J., Silliman, N., Peters, B.A., van der Heijden, M.S., et al. (2004). Mutational Analysis of the Tyrosine Phosphatome in Colorectal Cancers. Science *304*, 1164–1166. https://doi.org/10.1126/science.1096096.
26. Harman, J.R., Thorne, R., Jamilly, M., Tapia, M., Crump, N.T., Rice, S., Beveridge, R., Morrissey, E., de Bruijn, M.F.T.R., Roberts, I., et al. (2021). A KMT2A-AFF1 gene regulatory network highlights the role of core transcription factors and reveals the regulatory logic of key downstream target genes. Genome Res. *31*, 1159–1173. https://doi.org/10.1101/gr.268490.120.
27. Drews, R.M., Hernando, B., Tarabichi, M., Haase, K., Lesluyes, T., Smith, P.S., Morrill Gavarró, L., Couturier, D.-L., Liu, L., Schneider, M., et al. (2022). A pan-cancer compendium of chromosomal instability. Nature *606*, 976–983. https://doi.org/10.1038/s41586-022-04789-9.
28. McGranahan, N., and Swanton, C. (2017). Clonal Heterogeneity and Tumor Evolution: Past, Present, and the Future. Cell *168*, 613–628. https://doi.org/10.1016/j.cell.2017.01.018.
29. Bakhoum, S.F., Kabeche, L., Wood, M.D., Laucius, C.D., Qu, D., Laughney, A.M., Reynolds, G.E., Louie, R.J., Phillips, J., Chan, D.A., et al. (2015). Numerical chromosomal instability mediates susceptibility to radiation treatment. Nat. Commun. *6*, 5990. https://doi.org/10.1038/ncomms6990.
30. Zaki, B.I., Suriawinata, A.A., Eastman, A.R., Garner, K.M., and Bakhoum, S.F. (2014). Chromosomal instability portends superior response of rectal adenocarcinoma to chemoradiation therapy. Cancer *120*, 1733–1742. https://doi.org/10.1002/cncr.28656.
31. Bakhoum, S.F., Kabeche, L., Murnane, J.P., Zaki, B.I., and Compton, D.A. (2014). DNA-Damage Response during Mitosis Induces Whole-Chromosome Missegregation. Cancer Discov. *4*, 1281–1289. https://doi.org/10.1158/2159-8290.CD-14-0403.
32. van Jaarsveld, R.H., and Kops, G.J.P.L. (2016). Difference Makers: Chromosomal Instability versus Aneuploidy in Cancer. Trends Cancer *2*, 561–571. https://doi.org/10.1016/j.trecan.2016.09.003.
33. Kocakavuk, E., Anderson, K.J., Varn, F.S., Johnson, K.C., Amin, S.B., Sulman, E.P., Lolkema, M.P., Barthel, F.P., and Verhaak, R.G.W. (2021). Radiotherapy is associated with a deletion signature that contributes to poor outcomes in patients with cancer. Nat. Genet. *53*, 1088–1096. https://doi.org/10.1038/s41588-021-00874-3.
34. Ghandi, M., Huang, F.W., Jané-Valbuena, J., Kryukov, G.V., Lo, C.C., McDonald, E.R., Barretina, J., Gelfand, E.T., Bielski, C.M., Li, H., et al. (2019). Next-generation characterization of the Cancer Cell Line Encyclopedia. Nature *569*, 503–508. https://doi.org/10.1038/s41586-019-1186-3.
35. Bakker, B., Taudt, A., Belderbos, M.E., Porubsky, D., Spierings, D.C.J., de Jong, T.V., Halsema, N., Kazemier, H.G., Hoekstra-Wakker, K., Bradley, A., et al. (2016). Single-cell sequencing reveals karyotype heterogeneity in murine and human malignancies. Genome Biol. *17*, 115. https://doi.org/10.1186/s13059-016-0971-7.
36. Kester, L., de Barbanson, B., Lyubimova, A., Chen, L.-T., van der Schrier, V., Alemany, A., Mooijman, D., Peterson-Maduro, J., Drost, J., de Ridder, J., and van Oudenaarden, A. (2022). Integration of multiple lineage measurements from the same cell reconstructs parallel tumor evolution. Cell Genom. *2*, 100096. https://doi.org/10.1016/j.xgen.2022.100096.
37. van de Wetering, M., Francies, H.E., Francis, J.M., Bounova, G., Iorio, F., Pronk, A., van Houdt, W., van Gorp, J., Taylor-Weiner, A., Kester, L., et al. (2015). Prospective Derivation of a Living Organoid Biobank of Colorectal Cancer Patients. Cell *161*, 933–945. https://doi.org/10.1016/j.cell.2015.03.053.
38. Fujii, M., Shimokawa, M., Date, S., Takano, A., Matano, M., Nanki, K., Ohta, Y., Toshimitsu, K., Nakazato, Y., Kawasaki, K., et al. (2016). A Colorectal Tumor Organoid Library Demonstrates Progressive Loss of Niche Factor Requirements during Tumorigenesis. Cell Stem Cell *18*, 827–838. https://doi.org/10.1016/j.stem.2016.04.003.
39. de Leng, W.W.J., Gadellaa-van Hooijdonk, C.G., Barendregt-Smouter, F.A.S., Koudijs, M.J., Nijman, I., Hinrichs, J.W.J., Cuppen, E., van Lieshout, S., Loberg, R.D., de Jonge, M., et al. (2016). Targeted Next Generation Sequencing as a Reliable Diagnostic Assay for the Detection of Somatic Mutations in Tumours Using Minimal DNA Amounts from Formalin Fixed Paraffin Embedded Material. PLoS One *11*, e0149405. https://doi.org/10.1371/journal.pone.0149405.
40. Rousseeuw, P.J. (1987). Silhouettes: A graphical aid to the interpretation and validation of cluster analysis. J. Comput. Appl. Math. *20*, 53–65. https://doi.org/10.1016/0377-0427(87)90125-7.
41. Sondka, Z., Bamford, S., Cole, C.G., Ward, S.A., Dunham, I., and Forbes, S.A. (2018). The COSMIC Cancer Gene Census: describing genetic dysfunction across all human cancers. Nat. Rev. Cancer *18*, 696–705. https://doi.org/10.1038/s41568-018-0060-1.
42. Bolhaqueiro, A.C.F., Ponsioen, B., Bakker, B., Klaasen, S.J., Kucukkose, E., van Jaarsveld, R.H., Vivié, J., Verlaan-Klink, I., Hami, N., Spierings, D.C.J., et al. (2019). Ongoing chromosomal instability and karyotype evolution in human colorectal cancer organoids. Nat. Genet. *51*, 824–834. https://doi.org/10.1038/s41588-019-0399-6.
43. Beroukhim, R., Mermel, C.H., Porter, D., Wei, G., Raychaudhuri, S., Donovan, J., Barretina, J., Boehm, J.S., Dobson, J., Urashima, M., et al. (2010). The landscape of somatic copy-number alteration across human cancers. Nature *463*, 899–905. https://doi.org/10.1038/nature08822.
44. Corsello, S.M., Nagari, R.T., Spangler, R.D., Rossen, J., Kocak, M., Bryan, J.G., Humeidi, R., Peck, D., Wu, X., Tang, A.A., et al. (2020). Discovering the anticancer potential of non-oncology drugs by systematic viability profiling. Nat. Cancer *1*, 235–248. https://doi.org/10.1038/s43018-019-0018-6.

STAR★METHODS

KEY RESOURCES TABLE

REAGENT or RESOURCE	SOURCE	IDENTIFIER
Chemicals, peptides, and recombinant proteins		
Disapse II	Roche	12273600
TrypLE™ Express Enzyme	ThermoFisher	12604013
BME	Amsbio	3533-010-02
Organoid culture medium	This study	Table S6
ROCK inihbitor (Y-26732)	Tocris	1254
Gibco™ Recovery™ Cell Culture Freezing Medium	Gibco	12648010
Proteinase K (Ambion)	Invitrogen	AM2546
NlaIII	New England Biolabs	R0125S
T4 DNA ligase	New England Biolabs	M0202S
T4 DNA ligase reaction buffer	New England Biolabs	B0202S
ATP	Invitrogen	AM8110G
Critical commercial assays		
DNeasy Blood en Tissue Kits	QIAGEN	69504
CellTiter-Glo® 3D Cell Viability Assay	Promega	G9681
Deposited data		
Single cell DNA sequencing	This study	NCBI Sequence Read Archive accession number: PRJNA1015247
CCLE database: metadata	https://depmap.org	sample_info.csv (22Q2 release)
CCLE database: radiation sensitivity data	Yard et al. (https://doi.org/10.1038/ncomms11428)[15]	Supplementary Data 1
CCLE database: segment level copy number data	https://depmap.org	CCLE_segment_cn.csv (22Q2 release)
CCLE database: ABSOLUTE copy number, poidy and whole genome duplication calls	https://depmap.org Ghandi et al. (https://doi.org/10.1038/s41586-019-1186-3)[34]	CCLE_ABSOLUTE_combined_20181227.xlsx Copy_Number_(Absolute).csv
COSMIC cancer genes	https://cancer.sanger.ac.uk/census	N/A
Experimental models: Cell lines		
Rectal cancer patient-derived organoids	This study	TcBio#12-09
Software and algorithms		
AneuFinder	https://bioconductor.org Bakker et al. (https://doi.org/10.1186/s13059-016-0971-7)[35]	N/A
MEDICC2	https://bitbucket.org Kaufmann et al. (https://doi.org/10.1186/s13059-022-02794-9)[23]	N/A
snakemake	https://github.org Kester et al. (https://doi.org/10.1016/j.xgen.2022.100096)[36]	N/A
R (version 4.2.1)	https://cran.r-project.org	N/A
CINSignatureQuantification	https://github.org Drews et al., (https://doi.org/10.1038/s41586-022-04789-9)[27]	N/A

RESOURCE AVAILABILITY

Lead contact

Further information and requests for resources and reagents should be directed to and will be fulfilled by the lead contact, Onno Kranenburg (o.kranenburg@umcutrecht.nl).

Materials availability

Patient-derived organoids may be obtained from the lead contact with a completed materials transfer agreement.

Data and code availability

The raw sequencing data have been deposited at NCBI Sequence Read Archive and are publicly available under accession number PRJNA1015247. Code to reproduce the analyses and figures is available at https://github.com/dshandel/subclonal_evolution_paper (Zenodo https://doi.org/10.5281/zenodo.10432290). Any additional information required to reanalyze the data reported in this paper is available from the lead contact upon request.

EXPERIMENTAL MODEL AND SUBJECT PARTICIPANT DETAILS

Patient-derived tissue and clinical data

Written informed consent was obtained from all patients for the research use of their tissue and processing of clinical data, following the HUB biobank protocol HUB-cancer TcBio#12-09. Clinical data, including pTNM stage, (*neo*)adjuvant therapies, progression-free survival and overall survival from the time of surgical resection, were extracted by an independent data manager using a custom query. All clinical data accessible to the researchers were fully anonymized. The study was approved by the ethical review board of the University Medical Center Utrecht.

Patient-derived tumor organoid culturing

Rectal cancer patient-derived organoids were derived and cultured according to previously published protocols.[37,38] In brief, organoids were cultured in colorectal cancer culture medium consisting of advanced DMEM/F12 medium (Invitrogen) with supplements as detailed in Table S6. Tumor organoids were passaged by dissociating them with TrypLE (Gibco) for 5 min, followed by embedding them in a mixture of Basement Membrane Extract (BME; Amsbio) and culture medium in a 3:1 ratio. The resulting tumor organoids were then replated in drops of approximately 10 μL each, in a pre-warmed 6-well plate. To prevent anoikis, ROCK inhibitor (Y-27632, Tocris) at a concentration of 10 μM was added to the culture medium for 2 days.

METHOD DETAILS

Radiation response assays

To model radiation resistance, we adapted a previously published medium-throughput radiation dose response assay for compatibility with 3D organoid technology.[14,15] Five hundred three-day old organoids were embedded in a mixture of BME matrix and culture medium and plated in a 96-well plate as 4 μL droplets, thus allowing growth in 3D structures. Three hours later, organoids were irradiated with a single dose of 0–8 Gy using a linear accelerator (Elekta Precise Linear Accelerator 11F49 or Elekta Synergy Agility Linear Accelerator) with a separate plate used for each dose. To allow for photon scattering, the plates were placed on top of a 2-cm polystyrene board. After seven days, cell viability was assessed using CellTiter-Glo 3D (Promega), which is specifically validated for 3D microtissue cultures. The dose response data was normalized to 0 Gy, and then the area under the curve was calculated based on this normalized data. To standardize the area under the curve, it was divided by the maximum possible area that a curve could occupy.

Bulk genome sequencing

Whole exome sequencing data of HUB015 was obtained from the HUB foundation. Targeted next generation sequencing,[39] DNA was extracted using the DNeasy Blood en Tissue Kits (QIAGEN, 69504), according to the manufacturer's instructions (spin column protocol). Next, 20 ng of DNA extracted from organoid samples was used for sequencing, utilizing the Cancer Hotspot Panel v2 (Thermo Fisher); with some additional hotspots. Sequencing was carried out on the Ion Chef System (Thermo Fisher) and the IonTorrent S5 sequencer (Thermo Fisher), resulting in an average sequencing depth of 500x.

Subclonal evolution modeling

To assess subclonal evolution in response to radiation therapy, 250,000 single cells were plated in a 6-well plate and exposed to either 0 or 10 Gy of radiation three days later. In the treatment group (10 Gy), 'recurrence' was defined as the regrowth of cancer cells to a sufficient extent that allowed for subsequent passaging of the cells. Organoids were processed for single-cell whole genome sequencing 7 days after the first passage. The control group (0 Gy) was passaged every week.

Single-cell whole genome sequencing

Organoids were dissociated into single cells with TrypLE (Gibco). After washout of TrypLE, cells were frozen in 500 μL of recovery cell culture freezing medium (Gibco) for subsequent sorting and sequencing. G1 single nuclei, identified by propidium iodide and Hoechst staining, were sorted into a 384-well plate with 10 μL of mineral oil (Sigma-Aldrich) in each well, and stored at −80 °C. Cell lysis was carried out for 2 h at 50 °C using Proteinase K (Ambion) in 1x Cutsmart (New England Biolabs), followed by heat inactivation at 80 °C for 15 min. Genomic DNA was then fragmented with 100 nL of 1 U NlaIII (New England Biolabs) in 1× Cutsmart (New England Biolabs) for 2 h at 37 °C, followed by heat inactivation at 65 °C for 20 min. Next, the following was added to each well: (i) 50 nL containing 50 mM barcoded double-stranded NLAIII adapters; (ii) 150 nL of 1× T4 DNA ligase buffer containing 40 U T4 DNA ligase (New England Biolabs), supplemented with 10 mM ATP (Invitrogen). The mixture was ligated overnight at 16 °C, after which samples were pooled. Libraries were sequenced on an Illumina Nextseq 2000 with 2 x 100/150-bp paired-end sequencing.

Single-cell sequencing data processing

Preprocessing and quality selection

The sequencing data was processed using the *snakemake* workflows in Python (v. 3.6).[36] The cell barcodes were extracted and trimmed, and reads without NlaIII sequence or PCR-duplicated reads were removed. The trimmed reads were then mapped to hg38 using BWA 0.7.16a-r1181. R package 'AneuFinder' (v. 1.26.0) was used for GC correction, blacklisting of artefact-prone regions and copy number calling.[35] Copy numbers were called using the edivisive algorithm with variable width bins (mean 0.5 Mb) based on mappability. Following the removal of cells with high bin-to-bin variation (>0.7 spikiness) and cells with too few reads, a total of 2,994 high-quality cells remained, exhibiting an average of 26.9 ± 11.7 unique copy number alterations per cell.

Clustering of subclones

To create the clustering heat maps, Euclidean distances were calculated from the copy number state measurements with R's inbuilt 'dist and 'hclust' functions using wrapper functions from package 'AneuFinder'. For each individual organoid, the matrices containing copy number values before and after radiation were used to perform principal component analysis. Principal component 1 and principal component 2 were plotted on the x and y axes, respectively. As such, each dot in the principal component plots represents a single-cell copy number profile and is colored either by radiation status or by subclone group. The optimum number of subclones was defined by performing k-means clustering on the first 10 principal components and selecting the maximum average silhouette (*s*) width:

$$s(i) = \frac{b(i) - a(i)}{\max\{a(i), b(i)\}}$$

Where *a(i)* is the average intra-cluster distance and *b(i)* is the average inter-cluster distance.[40] Clusters that were separated on a principal component explaining more than 10% were defined as major subclones. Clusters that were separated on a principal component explaining less than 10% were labeled as minor subclones (e.g., HUB015, HUB005). If the silhouette method suggested multiple clusters, but no separated clusters could be identified on the principal component, this was dismissed as being a true subclone if the principal component explained less than 10% of the variance. Using this approach, the following k values were used: HUB183 (k = 1), HUB005 (k = 3), HUB015 (k = 3), HUB106 (k = 3), HUB062 (k = 3), and HUB197 (k = 3).

Phylogenetic trees were inferred from unphased copy number calls using MEDICC2 using default settings.[23] MEDICC2 infers phylogenies from copy number alterations based on the minimum-event distance (MED). Cells at baseline and recurrence were combined.

Subclonal expansion was defined as a significant 10-fold increase in the relative dominance of subclones, accompanied by the rejection of the null hypothesis of Fisher's exact test (thus indicating that the relative proportions of the subclones are dependent on the radiation status). Subclonal extinction referred to the total disappearance of subclones. Finally, subclonal persistence was defined as the maintenance of subclonal composition with minimal changes (less than 10-fold) before and after radiation.

Resistance-specific copy number analysis

Consensus copy number profiles of subpopulations (either whole organoids or subclones within organoids) were calculated using custom scripts. A copy number alteration was considered as 'consensus' when present in more than 60–80% of cells. To identify resistance-specific copy number alterations, consensus profiles of resistant subclones were compared to consensus profiles of sensitive subclones. Resistant subclones were defined as subclones that either persisted or expaned upon irradiation. To ensure specificity, a copy number alteration was deemed 'resistance-specific' only if present in more than 80% of resistant subclones, and in less than 10% of the sensitive subclones. All subclones within HUB015 (diploid) and whole-genome duplicated subclones within HUB197 were excluded from this analysis. COSMIC cancer gene census oncogenes were downloaded from https://cancer.sanger.ac.uk/census and mapped to each copy number alteration.[41]

Copy number pattern analysis

Heterogeneity was defined as

$$H = \frac{1}{TN}\sum_{n=1}^{N}\sum_{f=0}^{S} fm_{f,t}$$

where T and N sets containing bins and single cells, respectively.[42] S represents the total number of possible copy number states, while $m_{f,t}$ denotes the number of cells with a particular copy number s at bin t. Copy number transitions were shifted to a single shared middle position, thereby avoiding an overestimation of heterogeneity due to technical issues that cause shifts of copy number states transitions.[42] Intraclone variability was calculated from the pairwise distance matrix outputted by MEDICC2,[23] by calculating the average of the cell-to-cell distances within each subclone.

For copy number length analysis, each copy number alteration was standardized by dividing its length by the length of its corresponding chromosome arm. As such, a value of 1 indicated an alteration spanning an entire arm, while 2 indicated a whole-chromosome alteration. If the alteration spanned the centromere, the fractions for each arm were summed. Alterations were categorized as focal if their length value was less than 0.3, as large if their length value was between 0.3 and 0.98, and as arm to whole-chromosome level if their length value was greater than 0.98.[43]

Whole genome doubling and ploidy calls

Cancer cells from the Cancer Cell Line Encyclopedia (CCLE) were previously analyzed using the ABSOLUTE algorithm,[34] and downloaded from https://depmap.org. ABSOLUTE utilizes copy number and mutation data to calculate sample ploidy and whole genome doublings. Whole genome doubling status is inferred from the ploidy distribution within a specific tumor type, homologous copy number information across the genome, and the presence of duplicated mutations.[19] *In vitro* radiation response data of CCLE cell lines were obtained from Yard et al.[15] Whole genome duplication events were inferred from single cell data using MEDICC2.[23]

Chromosomal instability signature

Segment level copy number data ('CCLE_segment_cn.csv') from the CCLE database were downloaded from https://depmap.org.[34,44] We used the 22Q2 DepMap release. Chromosomal instability signatures scores were computed using the 'quantifyCNSignatures' package, with default settings.[27] This wrapper function computes signature scores for 17 chromosomal instability signatures, each having a unique putative cause.[27]

QUANTIFICATION AND STATISTICAL ANALYSIS

R version 4.2.1 was used for statistical analysis. Continuous variables were compared using the Mann–Whitney *U* test or Student's *t*-test/Welch Two Sample *t* test, where appropriate. Categorical variables were compared using Fisher's exact test. To compare signature/ploidy scores, or whole genome doubling status between the top radioresistant and radiosensitive CCLE lines, a linear or logistic model was fitted using the 'lm' or 'glm' package in R, using the following formula:

$$\textbf{CX signature score} \;/\; \textbf{ploidy} \;/\; \textbf{wgd status} \sim \textbf{resistancy group} + \textbf{primary cancer type} + \textbf{cancer subtype}$$

In the case of multiple comparisons *p* values were adjusted using the Bonferroni procedure.